npj | quantum materials

Article

Published in partnership with Nanjing University

https://doi.org/10.1038/s41535-026-00866-8

A wide-range topological thermometer with $Ta_2Pd_3Te_5$: from power-law response to application prospects

Yupeng Li[1,2,6], Anqi Wang[2,3,6], Senyang Pan[4], Dayu Yan[2], Guang Yang[2], Xingchen Guo[2,3], Yu Hong[2,3], Zhiyuan Zhang[2,3], Ziwei Dou[2], Guangtong Liu[2,5], Fanming Qu[2,3,5], Zhijun Wang[2,3], Tian Qian[2,5], Jinglei Zhang[4] ✉, Youguo Shi[2,5] ✉, Li Lu[2,3,5] ✉ & Jie Shen[2,5] ✉

In recent decades, there has been a persistent pursuit of applications for surface/edge states in topological systems, driven by their dissipationless transport effects. This work demonstrates the remarkable properties of the topological material $Ta_2Pd_3Te_5$, as a thermometer. At low temperatures, it shows a power-law correlation in temperature-dependent resistance, while behaving like a semiconductor at high temperatures. This dual behavior effectively mitigates the issue of infinite resistance in semiconductor thermometers at ultra-low temperatures, making it ideal for millikelvin-range refrigerators. Through chemical doping, thickness adjustment, and gate voltage control, its performance can be finely tuned, and can also enable micron-scale local temperature measurement from millikelvin to room temperature. Furthermore, this thermometer exhibits excellent temperature sensitivity and resolution, and can be fine-tuned to show small magnetoresistance. In summary, the $Ta_2Pd_3Te_5$-based thermometer, also referred to as a topological thermometer, demonstrates considerable potential for broad-temperature-range detection and merits further investigation and optimization.

Topological materials and physics have become a prominent field in condensed matter physics due to the emergence of various novel physical phenomena and the dissipationless transport features of topological surface/edge states[1–3]. The potential applications of these topological properties, such as topological electronic devices[4–7] and topological quantum computations[8,9], continue to be actively pursued. However, they either require further research to fully understand their capabilities or seem not to have yet demonstrated significant technological advantages compared to current technologies. In this context, a novel property of topological materials has been developed as a resistance thermometer for wide-range thermometry, representing a notable application for topological materials and potentially referred to as a topological thermometer.

The resistance thermometer, with its ability to measure a wide temperature range from millikelvin temperatures or below to room temperature, has gained increasing significance in the field of low-temperature physics. It plays a crucial role in efficiently studying successive phase transitions, particularly those involving ultra-low-temperature exotic quantum states such as the fractional quantum Hall effect[8], anomalous quantum Hall effect[10], quantum spin liquid[11], quantum phase transitions[12,13], non-Abelian anyons[14], and quantum states for quantum computing[15], among others. Although refrigerators supporting sub-mK temperatures or lower have been successfully developed for various types of experimental measurements[16–18], their widespread adoption is challenging due to the complex operations and inherent disadvantages. One important disadvantage is that thermometers such as the He-3 melting pressure thermometer[17,19], Coulomb blockade thermometry[16,20], noise thermometry[18,21], and pulsed platinum NMR thermometer[18,22,23], host complex preparation requirements and most of them are quite time-consuming for measuring ultra-low temperatures. On the contrary, semiconductor thermometers are extensively employed at low temperatures due to their high sensitivity and active feedback temperature control, as depicted in Fig. 1a. The semiconducting feature with a negative temperature

[1]Hangzhou Key Laboratory of Quantum Matter, School of Physics, Hangzhou Normal University, Hangzhou, China. [2]Beijing National Laboratory for Condensed Matter Physics, Institute of Physics, Chinese Academy of Sciences, Beijing, China. [3]School of Physical Sciences, University of Chinese Academy of Sciences, Beijing, China. [4]Anhui Province Key Laboratory of Condensed Matter Physics at Extreme Conditions, High Magnetic Field Laboratory of the Chinese Academy of Sciences, Hefei, Anhui, China. [5]Songshan Lake Materials Laboratory, Dongguan, China. [6]These authors contributed equally: Yupeng Li, Anqi Wang.
✉e-mail: zhangjinglei@hmfl.ac.cn; ygshi@iphy.ac.cn; lilu@iphy.ac.cn; shenjie@iphy.ac.cn

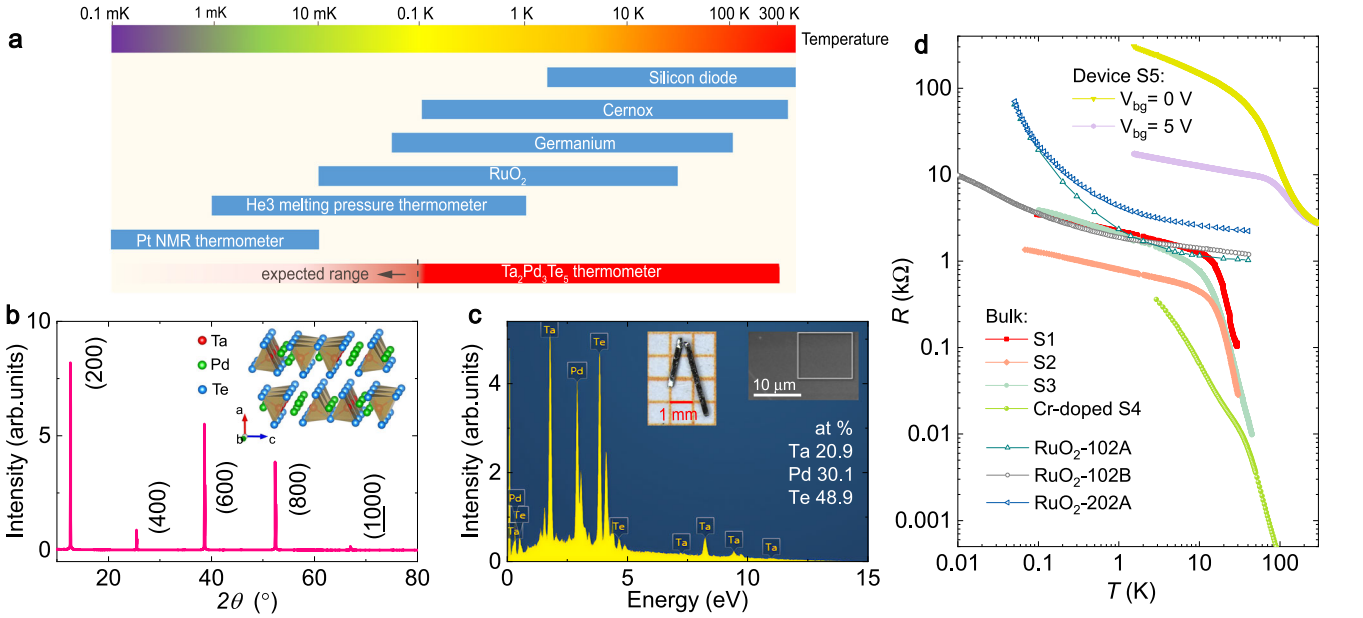

Fig. 1 | Properties of $Ta_2Pd_3Te_5$. a The temperature range application for various low-temperature thermometers. The blue bars represent commonly used commercial thermometers, while the left part of the dashed line in the $Ta_2Pd_3Te_5$ thermometer signifies its the predictable ability and requires further measurements. The temperature color bar scale is logarithmic. **b** Typical XRD spectrum for the (l00) facet of the single crystal. The inset displays the structure of the van der Waals material with quasi-one-dimensional (quasi-1D) Ta-Te chains. **c** Typical EDS spectra, which were collected on the flat clean surface, are shown in the right inset. The left inset displays the photomicrograph of the crystals. **d** Electrical resistance of pristine undoped and Cr-doped $Ta_2Pd_3Te_5$ bulk thermometers (S1–S4), thin-film $Ta_2Pd_3Te_5$ thermometer (S5), and RuO_2 thermometers[26].

coefficient causes the resistance (R) to increase exponentially as the temperature (T) decreases. Nevertheless, the giant resistance exhibited at millikelvin temperatures renders most semiconductor thermometers unusable. Consequently, temperature detection ranges and R–T curves of thermometers can be modulated by various methods, including controlling the ratio of conducting zirconium nitride to insulating zirconium oxide for Cernox thermometers[24], and adjusting the RuO_2 grain size and the volume fraction of RuO_2 in the paste for RuO_2 thermometers[25]. However, the capability to detect a broad temperature range is often constrained by limited measurement ranges, as seen in conventional thermometers like the RuO_2 thermometer, which typically operates between 10 mK and 40 K[26], and Cernox thermometers, which cover a range of 100 mK to 420 K[26]. A common strategy employs multiple thermometers to cover diverse temperature ranges; however, different thermometers may exhibit slight inconsistencies in overlapping ranges. Consequently, developing a resistance thermometer that diverges from traditional semiconducting properties is essential, not only to push the limits of ultra-low temperature measurement but also to expand the overall temperature range. Such a thermometer would also advance research in successive phase transitions and temperature-dependent physical phenomena.

In this work, a topological insulator $Ta_2Pd_3Te_5$[27–29] is chosen as the main material for the potential resistance thermometer. The material exhibits several compelling properties, including excitonic insulator states[30–32] and edge states[28,31,33,34], which may contribute to the following practical applications. For example, the edge states of the film can be utilized in fabricating an interfering Josephson diode[34], which exhibits high diode efficiency at small magnetic fields (B) with ultra-low power consumption. On the other hand, its R–T curve at low temperature deviates from a high-temperature semiconductor behavior ($R \propto e^{\Delta/2k_BT}$) and instead shows a power-law behavior ($R \propto T^{-\alpha}$), where Δ is the semiconductor gap, k_B is the Boltzmann constant, and α is a power-law coefficient. The power-law behavior may originate from the Luttinger liquid (LL) of edge states at low temperatures[28,35], leading to a slower rate of resistance increase with decreasing temperature compared to the typical observation in a semiconductor. Hence, the unique properties of a $Ta_2Pd_3Te_5$ thermometer can be utilized for detecting lower temperatures, while retaining the traditional semiconductor behavior for high-temperature detection. The observed transport properties may be attributed to the coexistence of edge states and a fully gapped excitonic insulator phase, while a trivial semimetal/metal exhibits conventional metallic R–T behavior and cannot function as a reliable thermometer for ultra-low temperature measurements. In addition, the relative ease of fabrication and stable performance across various thicknesses further positions the $Ta_2Pd_3Te_5$ thermometer as a preferred option over other LL systems[36–40], like carbon nanotubes[36].

Results

Characterization of $Ta_2Pd_3Te_5$

Before introducing the $Ta_2Pd_3Te_5$ thermometer, we first characterize the $Ta_2Pd_3Te_5$ single crystal. In Fig. 1b, the typical X-ray diffraction (XRD) data exhibit good spectra for the (l00) facet of the single crystal, indicating the high quality of our samples. Fig. 1c displays a typical pattern of the energy-dispersive X-ray spectroscopy (EDS), and the chemical composition is Ta:Pd:Te = 2.09:3.00:4.87 (Ta:Pd:Te:Cr = 1.77:3.00:4.99:0.01) for the pristine undoped (chromium-doped) compounds. Despite the low content of chromium in Cr-doped samples, their distinct transport properties compared to pristine samples will indicate the effective Cr-doping, as shown in Supplementary Figs. S2–S4. Bulks and devices are synthesized or fabricated using the same method as described in the literatures[28,29].

Transport measurements are conducted to investigate the properties of $Ta_2Pd_3Te_5$ thermometers (Fig. 1d). The temperature-dependent resistance of bulk samples S1, S2, and S3 exhibits significant deviation from typical semiconductor behavior below 20 K, with slight variations in observed values and characteristics across samples attributable to differences in size and quality. Notably, this deviation is integrally shown in device S5 over a wide temperature range, leading to a power-law behavior at low temperatures. The power-law behavior can also be observed from dV/dI–V_{bias} curves, and the conductance can be well scaled, suggesting the presence of LL stemming from edge states[28]. This type of LL has also been observed in

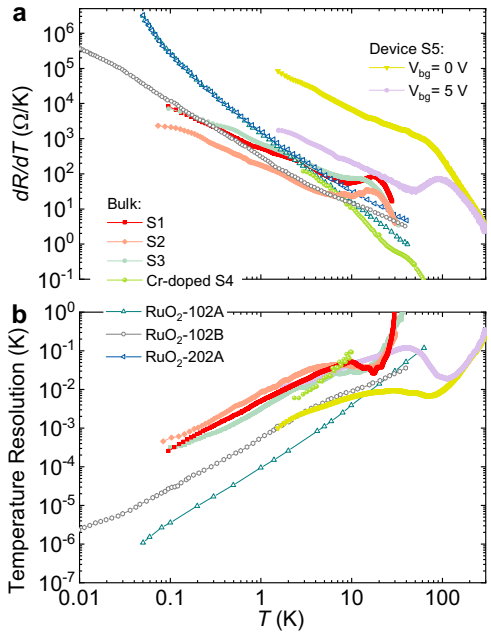

Fig. 2 | Temperature sensitivity and resolution. Temperature sensitivity (**a**) and resolution (**b**) for $Ta_2Pd_3Te_5$ thermometers and RuO_2 thermometers. The data for RuO_2 thermometers originate from literatures[26,42].

other 2D systems with edge states, such as quantum spin Hall insulators[37,38] and quantum Hall systems[39,40]. The power-law behavior provides a notable advantage, as it exhibits a much lower rate of resistance increase with decreasing temperature compared to the majority of commercial semiconductor thermometers[26,41] (Fig. 1d or Supplementary Fig. S1). For instance, commercial thermometers like RuO_2, germanium RTD, and Cernox can easily exceed 1 MΩ at temperatures below 100 mK, rendering them unusable at lower temperatures. Among these conventional semiconductor thermometers, RuO_2-102B[42] exhibits the smallest resistance at ultra-low temperature (Fig. 1d) and shows potential for lower temperature detection. Compared to RuO_2-102B, the $Ta_2Pd_3Te_5$ bulk thermometer easily possesses a much smaller increase rate of resistance at low temperature due to the small $\alpha \sim 0.21$, 0.21, and 0.31 for samples S1, S2, and S3, respectively. It also hosts a larger increase rate of resistance at high temperatures due to its excellent semiconductor behavior, in comparison to most RuO_2 thermometers, suggesting its high sensitivity at high temperatures. Therefore, it is an ideal candidate for wide-range temperature detection, particularly extending to ultra-low temperatures. The small Cr-doped $Ta_2Pd_3Te_5$ bulk shows low resistance at high temperatures, but it displays an approximate power-law behavior with a large α value of 1.55 (see Fig. 1d and Supplementary Fig. S2). This behavior suggests a comparable detection limit to RuO_2-102A and RuO_2-202A, because its projected resistance approaches the MΩ range at ~10 mK (see Supplementary Table SI).

Temperature sensitivity and resolution

The temperature sensitivity of $Ta_2Pd_3Te_5$ thermometers is further studied in Fig. 2a. The temperature sensitivity, which describes the resistance sensitivity of the thermometer to temperature, is typically small for semiconductor thermometers at high temperatures and significantly large at low temperatures. For bulk $Ta_2Pd_3Te_5$ thermometers, the sensitivity varies from ~10 (20 K) to 4×10^4Ω/K (0.1 K), comparable to that of the RuO_2-102B[42]. Their sensitivity remains substantial in the crossover region between power-law and semiconductor regimes but declines rapidly above 20 K as the system transitions progressively into a semiconductor state. In addition, the Cr-doped $Ta_2Pd_3Te_5$ thermometer also shows low sensitivity at high temperatures and high sensitivity at low temperatures (see Fig. 2a and Supplementary Fig. S2), indicating its better applicability at relatively low temperatures. Moreover, the thin-film thermometer (device S5) demonstrates higher resistance and sensitivity across a wider temperature range when compared to bulk thermometers and RuO_2 thermometers. These results demonstrate its suitable sensitivity for detecting a wider range of temperatures.

The temperature resolution of $Ta_2Pd_3Te_5$, defined as the minimum detectable temperature change during measurement[41], is also illustrated in Fig. 2b. This parameter can be expressed as $\Delta T = \Delta R/(dR/dT)$[26], where it depends on both the temperature sensitivity (dR/dT) and the instrument resistance resolution ΔR. The resolution is determined not only by the voltage noise level (U_n) of the measuring instrument but also by the applied current excitation (I_{ac}), with resistance resolution $\Delta R = U_n/I_{ac}$. In the case of instrument noise, several techniques, such as optimized filters, can be utilized to diminish system noise and improve measurement precision. Regarding the excitation, the application of a relatively large excitation in the circuit can also improve the measurement resolution. For instance, in our systems, multilevel filters are used to minimize the instrument noise U_n, to as low as ~10 nV, such as π filters in the measuring box, RC filters at the mixing chamber. The activation energy caused by applied current excitation I_{ac} is slightly lower than the thermal excitation energy at the given temperature, ensuring no noticeable Joule heating effect. Moreover, the lock-in technique (LI5650, NF Corporation, which offers the high precision measurement capabilities) is applied to provide the excitation and measure the thermometers. Compared to RuO_2-based thermometers, $Ta_2Pd_3Te_5$-based thermometers exhibit slightly lower temperature resolution at low temperatures (where smaller values indicate higher resolution, as shown in Fig. 2b), which maybe stem from the conservative estimation of ΔR. For bulk thermometers such as sample S1 at 0.1 K, the temperature resolution and precision (a ratio of temperature resolution to temperature) are lower than 0.3 mK and 0.3%, respectively. The thin-film thermometer S5 exhibits relatively high temperature resolution, highlighting its effectiveness for measuring temperatures across a wide range. Similarly, the Cr-doped sample S4 exhibits temperature resolution comparable to that of the pristine bulk sample at low temperatures, as shown in Fig. 2b and Supplementary Fig. S2. In summary, $Ta_2Pd_3Te_5$ film thermometers not only demonstrate exceptional capabilities for detecting a wide range of temperatures but also exhibit excellent temperature sensitivity and resolution.

Magnetoresistance

The $Ta_2Pd_3Te_5$ thermometers are subsequently calibrated under a magnetic field up to 31 T. The response of the thermometers to a magnetic field is also a crucial property, and their small magnetoresistance is beneficial for their applications. In Fig. 3a, the magnetoresistance [MR = $R(B)/R(0)-1$] of sample S2 could reach 29% (10%) at 31 T (9 T) and 1.8 K, consistent with the previously reported literature[43]. The MR is much smaller than that of many semimetals[44–48] and the germanium thermometer at low temperatures[26,49]. The temperature display error of the thermometer due to the presence of a magnetic field can be described by a ratio $\Delta T/T$[41] shown in Fig. 3b, where $\Delta T = |T(B) - T(0)|$. The value of $\Delta T/T$ at 1.8 K and 31 T is slightly over 70%, indicating a not small value compared to general thermometers. If considering a magnetic field strength of 9 T, it is estimated that $\Delta T/T(9\,\mathrm{T})$ is 41% at 1.8 K and 3.6% at 10.5 K, suggesting that the magnetic effect of the $Ta_2Pd_3Te_5$ thermometer can be considered negligible above 10 K.

In addition, angle-dependent magnetoresistance measurements are performed to study whether there is a small magnetoresistance at specific angles. In Fig. 3c, d, MR at 1.8 K for different angle θ shows a similar situation, with the smallest MR occurring at the perpendicular magnetic field $B_\perp$, which is the most commonly used direction in this material ($B_\perp \| a$ axis). MR at lower temperatures is further measured in sample S1, leading to slightly larger MR and $\Delta T/T$ in Fig. 3e, f.

The magnetoresistance of $Ta_2Pd_3Te_5$ thermometers can be effectively reduced by adjusting the Fermi level, for example, through chemical doping or voltage gating. The Cr-doped samples with higher carrier density exhibit a significant reduction in MR, with $\Delta T/T$ decreasing to as low as ~3% at 2 K

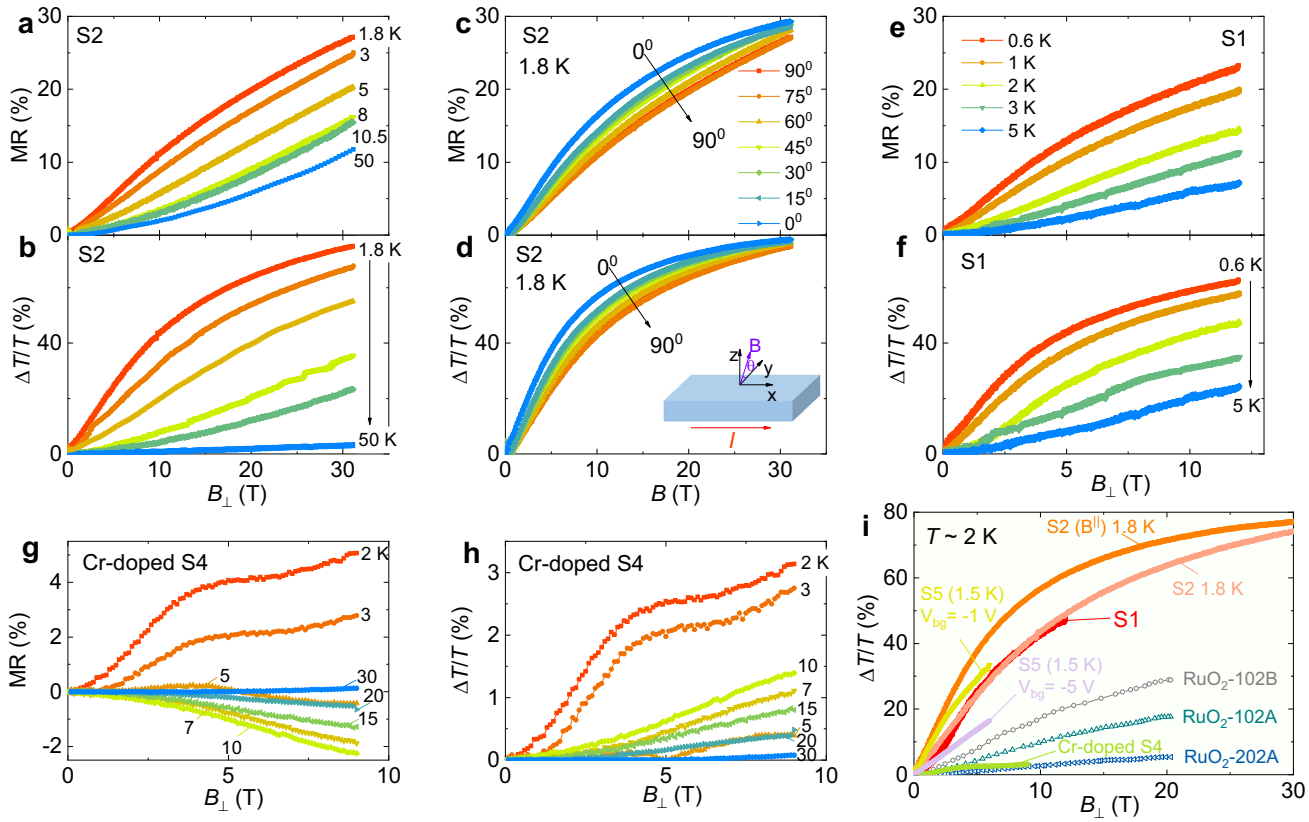

Fig. 3 | Magnetoresistance of $Ta_2Pd_3Te_5$ thermometers. MR of samples S2 (**a**), S1 (**e**), and Cr-doped S4 (**g**) at different temperatures. MR of the Cr-doped sample S4 is much smaller. **c** Slight anisotropic MR of sample S2. The change of temperature [$\Delta T = |T(B) - T(0)|$] under magnetic fields for samples S2 (**b**, **d**), S1 (**f**) and S4 (**h**). $\Delta T/T$ below 3 K for samples S4 and S5 is approximately estimated based on the extended power-law behavior of R –T curves. **i** Summary of $\Delta T/T$ (~2 K) under applied magnetic fields for $Ta_2Pd_3Te_5$ and commercial RuO_2[26] thermometers.

and 9 T, as shown in Fig. 3g, h, and Supplementary Figs. S3 and S4. This observation is further supported by additional samples S6 and S7 (refer to Supplementary Fig. S3). Its $\Delta T/T$ under a magnetic field can be comparable to that of the RuO_2-202A[26] (Fig. 3i), suggesting its strong applicability under magnetic fields and indicating its potential to replace the RuO_2-202A and several resistance thermometers at ultra-low temperatures. The reproducible measurements performed in three Cr-doped $Ta_2Pd_3Te_5$ thermometers highlight their high stability (see Supplementary Fig. S3). The thin-film thermometer also shows greater magnetoresistance than RuO_2 thermometers[26] (Fig. 3i), but its magnetoresistance can be greatly reduced when deviating from the charge neutral point (CNP), similar to the Cr-doped case.

Modulation of thin-film devices

To expand the thermometry range of $Ta_2Pd_3Te_5$ thermometers, the thin-film thermometer is a favorable option due to its relatively high resistance at high temperatures, suitable α at low temperatures, and excellent temperature sensitivity/resolution. The bulk thermometer, while performing well for ultra-low temperatures, seems not suitable for use above 30 K due to its low resistance and sensitivity, as illustrated in Figs. 1 and 2. Therefore, two methods are employed to overcome this shortcoming: thickness modulation and gate modulation. First, the thickness-dependent R–T curves at CNP are shown in Fig. 4a. At high temperatures, the large resistance (>~100 Ω) of the sensor is observed for thickness <100 nm, ensuring relatively high sensitivity. Thus, thin-film thermometers can readily extend the working temperature range up to 300 K. As for enhancing the measurement limit for ultra-low temperatures, there are two important factors to our knowledge. One contributing factor is the suitable transition temperature (T_1) that deviates from the typical behavior observed in semiconductors. In Fig. 4a, T_1 gradually decreases (indicated by the violet dashed line) with increasing thickness of $Ta_2Pd_3Te_5$ films, which has been previously discussed in our prior literature[28]. Another factor is the relatively small power-law coefficient α. Therefore, thin-film thermometers with an optimal thickness range (10 nm < thickness < 100 nm) exhibit excellent and stable performance, characterized by suitable α (Fig. 4b), resistance, and T_1. Moreover, their fabrication and application for a wide range of temperature detection can be easily achieved.

On the other hand, gate or carrier density modulation is an effective method for tuning the R–T curves of a film thermometer, particularly at low temperatures. For example, for sample S5, when the back gate voltage V_{bg} exceeds −4 or 5 V (using boron nitride as an insulator medium for the gate), as shown in Fig. 4c, the resistance gradually increases or even decreases as the temperature reduces, following a departure from the semiconducting behavior. Consequently, it begins to deviate from the favorable power-law behavior, although it may reenter an apparent power-law behavior at lower temperatures. The relatively good power-law behavior is observed within the large gating range ($-4\ V < V_{bg} < 5\ V$) in Fig. 4c. In Fig. 4d, α demonstrates similar variations to resistance in response to changes in V_{bg}. The reduction of α at the conduction band is consistent with the results in the SiO_2 gate-tuned α[28]. Therefore, by attaining an appropriate R–T curve and α near the CNP, it becomes possible to enable wide-range temperature detection (see Supplementary Table SI) and micron-scale localized temperature sensing.

Discussion

Before reaching a conclusion about this $Ta_2Pd_3Te_5$ thermometer, it is important to clarify several key aspects related to the low-temperature experiments. Heat capacity contributions arising from different

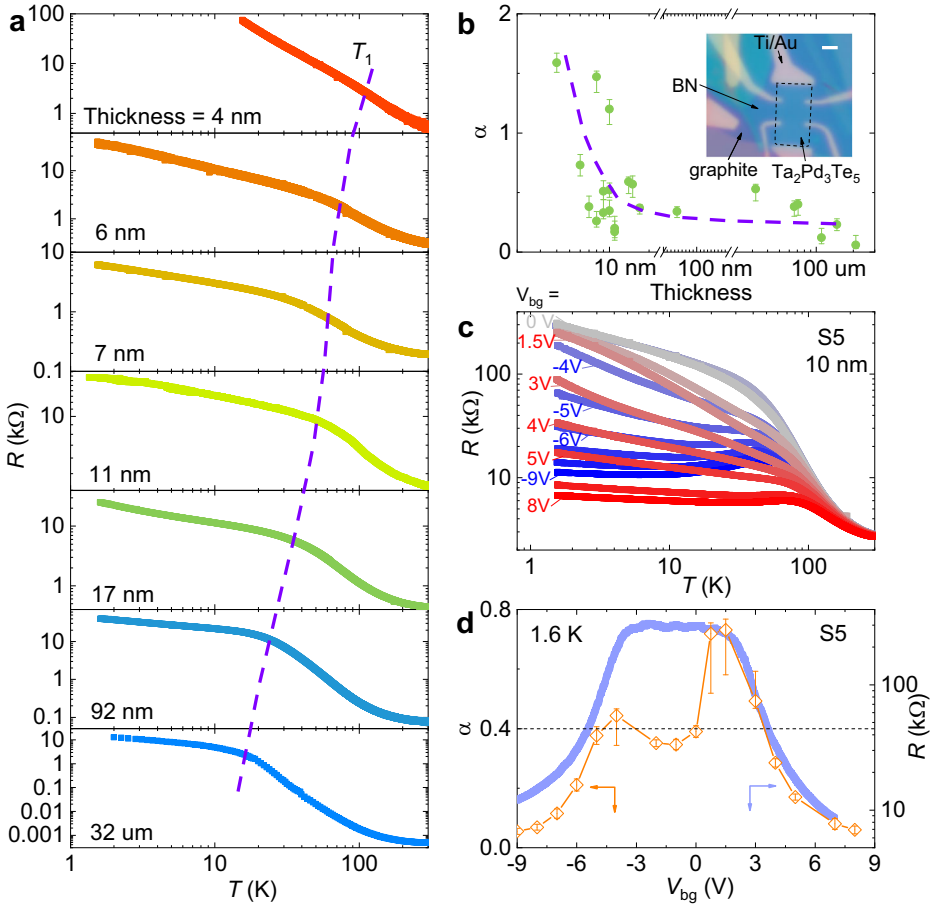

Fig. 4 | Thickness and gate-dependent resistance of $Ta_2Pd_3Te_5$. a Thickness dependence of R–T curves in $Ta_2Pd_3Te_5$ at CNP. The violet dashed line is the guideline for T_1. **b** α as a function of thickness. The inset shows a typical $Ta_2Pd_3Te_5$ device, with the white scale bar corresponding to 2 μm. The violet dashed line serves as the guideline for thickness-dependent α. **c** Temperature-dependent resistance at different V_{bg} for device S5. The relatively large resistance of device S5 at low T is primarily attributed to its small cross-sectional area. **d** V_{bg}-dependent resistance and α in sample S5. This device with $\alpha < 0.4$ seems more suitable to detect lower temperatures (Supplementary Table SI).

mechanisms in materials necessitate tailored cooling strategies at different temperature ranges. Taking copper[50], a commonly used material in low-temperature experiments, as an example, phonon heat capacity ($C_p \propto T^3$) dominates above 1 K, whereas electronic heat capacity ($C_p \propto T$) becomes dominant below ~1 K. At even lower temperatures (below ~1 mK), nuclear spin heat capacity begins to dominate the thermal properties. These indicate the complexity and difficulty of experiments conducted at millikelvin temperatures. Consequently, semiconductor-type thermometers face significant challenges at millikelvin temperatures, owing to both their near-infinite electrical resistance and the fundamental difficulty in achieving sufficient electron temperature reduction. It should be noted that the actual electron temperature of the sensor/chip in the refrigerator easily exceeds the millikelvin base temperature[51], primarily due to parasitic radiofrequency heating and self-heating effects. The former can be mitigated through multi-stage filtering, while the latter can be partially reduced by lowering the excitation current.

Furthermore, beyond external considerations, for a resistance thermometer to operate effectively at low temperatures, it must first maintain a resistance below the 1 MΩ level. In Table 1, Supplementary Table SI and Fig. S1, it is evident that general commercial semiconductor thermometers, such as Cernox, germanium RTD, RuO_2-102A, and RuO_2-202A, have extensional resistances much larger than 1 MΩ below ~10 mK, indicating their limited ability to effectively detect lower temperatures. Subsequently, RuO_2-102B was developed through the control of the proportion of RuO_2, paste, and other components[25], resulting in its resistance deviating distinctly from exponential response (Fig. 1d) at low temperatures[42,51]. Consequently, this form of RuO_2 enables temperature detection down to lower temperatures (Supplementary Table SI), although its upper detection limit is still confined to about 40 K. On the contrary, Cernox exhibits high temperature sensing capability, but its low-temperature operational limit remains relatively high above 0.1 K[26]. In addition, although $Ta_2Pd_3Te_5$ shows promising potential at low temperature due to its effective suppression of exponentially increasing resistance via power-law behavior, systematic characterization below 0.1 K remains to be conducted under specially optimized refrigeration configurations. This limitation arises because the electron temperature in our current cryogenic system cannot be effectively and timely cooled to such low temperatures, as shown in Supplementary Fig. S7.

Table 1 summarizes the performance characteristics of conventional low-temperature thermometers and $Ta_2Pd_3Te_5$-based thermometers. This material offers unique advantages for micron-scale local temperature measurements in 2D materials and nanodevices - a critical niche where conventional sensors face limitations. For instance, Cernox and RuO_2 thermometers are typically too bulky for such applications, while alternatives like Pt electrodes suffer from diminished sensitivity below 20 K. Moreover, the material demonstrates excellent measurement repeatability within 1 month (Supplementary Fig. S6), though extended-duration stability requires further evaluation in future commercial iterations. In addition, this thermometer exhibits three main limitations: (1) Pronounced MR in its pristine undoped form (Fig. 3i, Table 1); (2) Limited utility above 20 K for bulk samples due to rapidly declining sensitivity; (3) The gap remains between the current experimental results and commercial applications. A key challenge remains the scale-up of thin-layer sample production, particularly through sputtering techniques or alternative methods, while Cernox and RuO_2 have been commercialized and show excellent performance. In summary, although this class of topological thermometers demonstrates considerable potential for measuring a wider range of temperatures, further investigation is warranted to optimize their performance characteristics and fabrication processes.

Table 1 | Summary of properties for typical ultra-low temperature resistance thermometers

Thermometers	Suggested *T*-range	Δ*T*/*T* (2 K, 9 T)	Performance in *B*	*R*–*T* curve
Bulk TPT	0.1–20 K	40%	NS	PL+SC
Bulk Cr-TPT	0.1–20 K	3.1%	Good	PL+SC
Film TPT	0.1–300 K	>10%	Good (>10 K)	PL+SC
Cernox[26]	0.1–420 K	<6%	Good (>1 K)	SC
RuO_2-102B[26]	0.005–40 K	15%	NS	SC
RuO_2-102A[26]	0.05–40 K	~9%	Good	SC
RuO_2-202A[26]	0.05–40 K	2.5%	Good	SC
Ge RTD[26]	0.05–100 K	>60%	NS	SC

We abbreviate $Ta_2Pd_3Te_5$ as TPT, Cr-doped $Ta_2Pd_3Te_5$ as Cr-TPT, power law as PL, semiconductor as SC, and "not suggested" as NS. In column (Performance in *B*), we present the usage recommendations for TPT under high-*B* conditions, while the recommendations for other thermometers in *B* are obtained from the Lakeshore website[26]. *R*–*T* curve of TPT includes the PL and SC behavior.

Methods

Sample preparation and characterization

Single crystals of $Ta_2Pd_3Te_5$ and Cr-doped $Ta_2Pd_3Te_5$ were synthesized using the self-flux method[29]. The XRD data were collected by monochromatic Cu $K_{\alpha 1}$ radiation, and the composition ratio of the crystals was analyzed by EDS. The $Ta_2Pd_3Te_5$ devices were fabricated using conventional nanofabrication technology[28].

Transport measurements

The electrical resistance measurements at low magnetic fields were performed in Oxford TeslatronPT cryostats and dilution refrigerators, using constant voltage measurement methods. The Cr-doped samples are measured in the Physical Property Measurement System in the public performance, using the constant current measurement method. The resolution of Cr-doped samples is only displayed at low temperatures, as the discontinuous excitation current is applied during this measurement, and its low-temperature resolution is closer to the low-temperature limit. The high-field magnetotransport measurements were also performed using a standard AC lock-in technique with a DC-resistive magnet (~31 T) at the China High Magnetic Field Laboratory (CHMFL) in Hefei.

Data availability

The data within this paper are available from the corresponding author.

Received: 28 September 2025; Accepted: 5 February 2026;
Published online: 20 February 2026

References

1. Hasan, M. Z. & Kane, C. L. Colloquium: topological insulators. *Rev. Mod. Phys.* **82**, 3045–3067 (2010).
2. Armitage, N. P., Mele, E. J. & Vishwanath, A. Weyl and Dirac semimetals in three-dimensional solids. *Rev. Mod. Phys.* **90**, 015001 (2018).
3. Bernevig, B. A., Felser, C. & Beidenkopf, H. Progress and prospects in magnetic topological materials. *Nature* **603**, 41–51 (2022).
4. Brahlek, M. Criteria for realizing room-temperature electrical transport applications of topological materials. *Adv. Mater.* **32**, 2005698 (2020).
5. Gilbert, M. J. Topological electronics. *Commun. Phys.* **4**, 70 (2021).
6. Zhao, Y. et al. Anisotropic Fermi surface and quantum limit transport in high mobility three-dimensional Dirac semimetal Cd_3As_2. *Phys. Rev. X* **5**, 031037 (2015).
7. Munyan, S., Guo, B., Huynh, W., Huang, V. & Stemmer, S. Edge mode percolation and equilibration in the topological insulator cadmium arsenide. *npj Quantum Mater.* **8**, 70 (2023).
8. Nayak, C., Simon, S. H., Stern, A., Freedman, M. & Das Sarma, S. Non-Abelian anyons and topological quantum computation. *Rev. Mod. Phys.* **80**, 1083–1159 (2008).
9. He, M., Sun, H. & He, Q. L. Topological insulator: spintronics and quantum computations. *Front. Phys.* **14**, 43401 (2019).
10. Chang, C.-Z. et al. Experimental observation of the quantum anomalous Hall effect in a magnetic topological insulator. *Science* **340**, 167–170 (2013).
11. Zhou, Y., Kanoda, K. & Ng, T.-K. Quantum spin liquid states. *Rev. Mod. Phys.* **89**, 025003 (2017).
12. Vojta, M. Quantum phase transitions. *Rep. Prog. Phys.* **66**, 2069–2110 (2003).
13. Xing, Y. et al. Quantum Griffiths singularity of superconductor-metal transition in Ga thin films. *Science* **350**, 542–545 (2015).
14. Stern, A. Non-Abelian states of matter. *Nature* **464**, 187–193 (2010).
15. Steane, A. Quantum computing. *Rep. Prog. Phys.* **61**, 117–173 (1998).
16. Sarsby, M., Yurttagül, N. & Geresdi, A. 500 microkelvin nanoelectronics. *Nat. Commun.* **11**, 1492 (2020).
17. Yan, J., Yao, J., Shvarts, V., Du, R.-R. & Lin, X. Cryogen-free one hundred microKelvin refrigerator. *Rev. Sci. Instrum.* **92**, 025120 (2021).
18. Rothfuß, D., Reiser, A., Fleischmann, A. & Enss, C. Noise thermometry at ultra low temperatures. *Appl. Phys. Lett.* **103**, 052605 (2013).
19. Rusby, R. L. et al. The provisional low temperature scale from 0.9 mK to 1 K, PLTS-2000. *J. Low Temp. Phys.* **126**, 633 (2002).
20. Yurttagül, N., Sarsby, M. & Geresdi, A. Coulomb blockade thermometry beyond the universal regime. *J. Low Temp. Phys.* **204**, 143–162 (2021).
21. Lusher, C. P. et al. Current sensing noise thermometry using a low T_c DC SQUID preamplifier. *Meas. Sci. Technol.* **12**, 1–15 (2001).
22. Buchal, C., Hanssen, J., Mueller, R. M. & Pobell, F. Platinum wire NMR thermometer for ultralow temperatures. *Rev. Sci. Instrum.* **49**, 1360–1361 (1978).
23. Pobell, F. Nuclear refrigeration and thermometry at microkelvin temperatures. *J. Low Temp. Phys.* **87**, 635–649 (1992).
24. Courts, S. S. & Swinehart, P. R. Review of Cernox™ (zirconium oxynitride) thin-film resistance temperature sensors. *AIP Conf. Proc.* **684**, 393–398 (2003).
25. Zak, D. et al. Implementation of RuO_2-glass based thick film resistors in cryogenic thermometry. *Meas. Sci. Technol.* **17**, 22–27 (2006).
26. Lake Shore Cryotronics, Inc., USA. See https://www.lakeshore.com/.
27. Guo, Z., Deng, J., Xie, Y. & Wang, Z. Quadrupole topological insulators in $Ta_2M_3Te_5$ (M = Ni, Pd) monolayers. *npj Quantum Mater.* **7**, 87 (2022).
28. Wang, A. et al. A robust and tunable Luttinger liquid in correlated edge of transition-metal second-order topological insulator $Ta_2Pd_3Te_5$. *Nat. Commun.* **14**, 7647 (2023).
29. Guo, Z. et al. Quantum spin Hall effect in $Ta_2M_3Te_5$ (M =Pd,Ni). *Phys. Rev. B* **103**, 115145 (2021).
30. Huang, J. et al. Evidence for an excitonic insulator state in $Ta_2Pd_3Te_5$. *Phys. Rev. X* **14**, 011046 (2024).
31. Hossain, M. S. et al. Topological excitonic insulator with tunable momentum order. *Nat. Phys.* **21**, 1250–1259 (2025).
32. Zhang, P. et al. Spontaneous gap opening and potential excitonic states in an ideal Dirac semimetal $Ta_2Pd_3Te_5$. *Phys. Rev. X* **14**, 011047 (2024).
33. Wang, X. et al. Observation of topological edge states in the quantum spin Hall insulator $Ta_2Pd_3Te_5$. *Phys. Rev. B* **104**, L241408 (2021).
34. Li, Y. et al. Interfering Josephson diode effect in $Ta_2Pd_3Te_5$ asymmetric edge interferometer. *Nat. Commun.* **15**, 9031 (2024).
35. Guo, X. et al. Magnetic-field control of Tomonaga-Luttinger liquids in $Ta_2Pd_3Te_5$ edge states. Preprint at https://doi.org/10.48550/arXiv.2510.07973 (2025).
36. Bockrath, M. et al. Luttinger-liquid behaviour in carbon nanotubes. *Nature* **397**, 598–601 (1999).

37. Li, T. et al. Observation of a helical Luttinger liquid in InAs/GaSb quantum spin Hall edges. *Phys. Rev. Lett.* **115**, 136804 (2015).
38. Stühler, R. et al. Tomonaga-Luttinger liquid in the edge channels of a quantum spin Hall insulator. *Nat. Phys.* **16**, 47–51 (2020).
39. Chang, A. M., Pfeiffer, L. N. & West, K. W. Observation of chiral Luttinger behavior in electron tunneling into fractional quantum Hall edges. *Phys. Rev. Lett.* **77**, 2538–2541 (1996).
40. Hashisaka, M., Hiyama, N., Akiho, T., Muraki, K. & Fujisawa, T. Waveform measurement of charge- and spin-density wavepackets in a chiral Tomonaga-Luttinger liquid. *Nat. Phys.* **13**, 559–562 (2017).
41. Yeager, C. J. & Courts, S. S. A review of cryogenic thermometry and common temperature sensors. *IEEE Sens. J.* **1**, 352–360 (2001).
42. Courts, S. S. & Krause, J. K. A commercial ruthenium oxide thermometer for use to 20 millikelvin. *AIP Conf. Proc.* **985**, 947–954 (2008).
43. Jiao, W.-H. et al. Weak antilocalization in the transition metal telluride $Ta_2Pd_3Te_5$. *Phys. Rev. B* **108**, 245145 (2023).
44. Hu, J., Xu, S.-Y., Ni, N. & Mao, Z. Transport of topological semimetals. *Annu. Rev. Mater. Res.* **49**, 207–252 (2019).
45. Li, Y. et al. Quantum transport in a compensated semimetal W_2As_3 with nontrivial Z_2 indices. *Phys. Rev. B* **98**, 115145 (2018).
46. Li, Y. et al. Pressure-induced superconductivity in topological semimetal $NbAs_2$. *npj Quantum Meter.* **3**, 58 (2018).
47. Wang, Z. et al. Helicity-protected ultrahigh mobility Weyl fermions in NbP. *Phys. Rev. B* **93**, 121112(R) (2016).
48. Xu, Z. et al. Quasi-linear magnetoresistance and paramagnetic singularity in hypervalent bismuthide. *npj Quantum Mater.* **10**, 41 (2025).
49. Mitin, V. F., Dugaev, V. K. & Ihas, G. G. Large negative magnetoresistance in Ge films at ultralow temperatures and low magnetic fields. *Appl. Phys. Lett.* **91**, 202107 (2007).
50. Jones, A. T. et al. Progress in Cooling Nanoelectronic Devices to Ultra-Low Temperatures. *J. Low Temp. Phys.* **201**, 772–802 (2020).
51. Myers, S. A., Li, H. & Csáthy, G. A. A ruthenium oxide thermometer for dilution refrigerators operating down to 5 mK. *Cryogenics* **119**, 103367 (2021).

Acknowledgements

The authors acknowledge the support from the Synergetic Extreme Condition User Facility (SECUF), the Center for Materials Genome, and the China High Magnetic Field Laboratory (CHMFL) in Hefei. This work was supported by the Beijing Natural Science Foundation (Grant No. JQ23022), the National Natural Science Foundation of China (Grant Nos. 12404154, 92065203, U2032204, 11974395, 12188101 and 12122411), the Strategic Priority Research Program of Chinese Academy of Sciences (Grant Nos. XDB33000000 and XDB33030000), National Key Research and Development Program of China (Grant Nos. 2023YFA1607400 and 2024YFA1613200), the HZNU scientific research and innovation team project (Grant No. TD2025013), the National Key R&D Program of the MOST of China (Grant No. 2022YFA1602602), the Informatization Plan of Chinese Academy of Sciences (Grant No. CAS-WX2021SF-0102), the Beijing National Laboratory for Condensed Matter Physics (Grant No. 2025BNLCMPKF013), and the Zhejiang Provincial Natural Science Foundation of China (Grant No. LMS26A040010).

Author contributions

J.S. and Y.P.L. conceived and designed the experiment. Y.P.L. and A.Q.W. fabricated the devices with the assistance of G.Y., X.C.G., Z.Y.Z., and Y.H. Y.P.L. and A.Q.W. performed the transport measurements, supervised by T.Q., Z.W.D., G.T.L., F.M.Q., L.L., and J.S. S.Y.P. and J.L.Z. performed the high-field transport measurements. D.Y.Y. and Y.G.S. prepared $Ta_2Pd_3Te_5$ crystals. Z.J.W. provided the theoretical support. Y.P.L., A.Q.W. and J.S. wrote the manuscript with help from all other co-authors.

Competing interests

The authors declare no competing interests.

Additional information

Supplementary information The online version contains supplementary material available at https://doi.org/10.1038/s41535-026-00866-8.

Correspondence and requests for materials should be addressed to Jinglei Zhang, Youguo Shi, Li Lu or Jie Shen.